Physics Letters B 838 (2023) 137667

Contents lists available at ScienceDirect

Physics Letters B

journal homepage: www.elsevier.com/locate/physletb

Charmed meson production based on dipole transverse momentum representation in high energy hadron-hadron collisions available at the LHC

G. Sampaio dos Santos [a], G. Gil da Silveira [a,b,c,*], M.V.T. Machado [a]

[a] High Energy Physics Phenomenology Group, GFPAE IF-UFRGS, Caixa Postal 15051, CEP 91501-970, Porto Alegre, RS, Brazil
[b] CERN, PH Department, 1211 Geneva, Switzerland
[c] Departamento de Física Nuclear e de Altas Energias, Universidade do Estado do Rio de Janeiro, CEP 20550-013, Rio de Janeiro, RJ, Brazil

ARTICLE INFO

Article history:
Received 18 May 2022
Received in revised form 20 December 2022
Accepted 2 January 2023
Available online 11 January 2023
Editor: J.-P. Blaizot

Keywords:
Charmed meson
Proton-proton collisions
Saturation physics
Color dipole formalism

ABSTRACT

The production of D-mesons in high-energy pp collisions at the LHC kinematic regime is analyzed with the color dipole approach in the momentum representation. We present predictions for the D-meson differential cross section in terms of the transverse momentum and rapidity distributions taking into account the nonlinear behavior of the QCD dynamics. Comparison between our results and the corresponding experimental measurements reported by the ALICE and LHCb Collaborations in different rapidity bins is performed. We show that the D-meson production in the high energy limit can be properly addressed by using the QCD dipole transverse momentum distributions.

1. Introduction

The study of charmed mesons has been performed over the years, resulting in improvements on both experimental and theoretical fields, namely the production mechanism and the properties of such mesons are subjects of investigation. The charmed mesons are the lightest particles that have a heavy quark as its constituent, consequently, they can be a relevant tool to test theoretical frameworks regarding quarks and their interactions [1]. In particular, D-mesons were first observed in 1976 by experimental measurements performed by the SLAC-LBL Collaboration with the Mark I detector at the SPEAR collider at center-of-mass energies from 3.9 to 4.6 GeV [2,3]. The D-meson production was investigated in e^+e^- annihilation as well as in deep inelastic ep scattering (DIS), where the process directly probes the gluon distribution in the proton. Aiming the scenario of the heavy ion program at high-energy colliders, the study of the D-meson in pp collisions serves as a powerful baseline to investigate the cold nuclear matter effects as well as the effects originated in hot matter by a medium known as quark-gluon plasma (QGP) [4,5]. However, considering hadron-hadron collisions in the high energy regime, charm quarks are produced in the hard scattering processes between the initial-state partons present in the colliding hadrons. Subsequently, there is the hadronization process of these heavy quarks that originates the D-mesons in the final state. In particular, the operation of the Large Hadron Collider (LHC) – specially concerning the precision of the measurements plus a wide window of center-of-mass energy, transverse momentum, and rapidity – provides an interesting scenario to study charmed meson production. Transverse momentum and rapidity distributions probed at the LHC energies allow to investigate the D-meson production at small values of the Bjorken variable x, where significant nonlinear effects of the QCD regimes are expected. Therefore, the processes involving the open-meson production is expected to be sensitive to the nonlinear QCD dynamics. Hence, this particular kinematic region can be investigated with D-meson measurements at forward rapidities. The production cross section dependent on the detector kinematic variables is obtained by the scope of QCD calculations. The two most studied approaches consist of obtaining the differential cross section as function of the squared momentum transfer Q^2, known as collinear factorization [6], or in terms of the partonic transverse momentum k_T, namely k_T-factorization [7–10] formalism. For example, studies concerning heavy quarks together with heavy D mesons assuming collinear factorization can be found in the literature based on the general-mass variable-flavor-number scheme (GM-VFNS) [11,12], and in the fixed order plus next-to-leading logarithms approach (FONLL) [13,14]. On the other hand, calculations

* Corresponding author at: High Energy Physics Phenomenology Group, GFPAE IF-UFRGS, Caixa Postal 15051, CEP 91501-970, Porto Alegre, RS, Brazil.
E-mail address: gustavo.silveira@cern.ch (G. Gil da Silveira).

https://doi.org/10.1016/j.physletb.2023.137667

for heavy quark production in the k_T-factorization framework are available in Refs. [15–20]. Additionally, an analysis regarding the D-meson production including the intrinsic heavy quark component in the hadron wave function is performed in Refs. [21,22].

The k_T-factorization approach is applied to processes in hadron-hadron scattering at the high-energy limit and hard scattering matrix elements at small-x are calculated in such framework. In particular, one employs the gluon densities via the unintegrated gluon distribution (UGD). The gluon primordial transverse momentum distribution allows evaluating and extracting information concerning the properties of the structure of the proton, as well as the QCD evolution equations that take into account the transverse momentum of the partons. Moreover, the UGD is also a function of the momentum fraction x and the factorization scale μ_F^2. Such densities are not computed from first principles and need to be parametrized. There are in the literature various models for UGD which differ on underlying assumptions. Then, the observables strongly sensitive to the UGD need to be investigated in order to constrain the k_T-dependent distributions [23]. Within the k_T-factorization framework, the D-meson production cross section is obtained by the corresponding charm quark production process described in terms of UGD at small-x and at the scale $\mu_F \sim 2m_c$.

The D-meson production in high-energy processes (equivalently small-x) can be investigated within the color dipole formalism [24], which has been proven suitable to evaluate different processes in high energy phenomenology. In the color dipole framework the phenomenology is based on the universal dipole cross section that includes the nonlinear behavior and high-order corrections of the QCD dynamics [25]. The hard process is viewed in terms of $q\bar{q}$ dipole scattering off the target, namely the projectile emits a gluon that subsequently fluctuates into a $q\bar{q}$ color pair characterizing a color dipole with definite size which interacts with the color field of the target. The corresponding dipole amplitude is related to the intrinsic dipole k_T-distribution, i.e. the dipole transverse momentum distribution (TMD). In the limit of large gluon transverse momentum the dipole TMD corresponds approximately to the UGD. In the present investigation we consider analytical expressions for the TMDs based on parton saturation physics.

In this work, based on the theoretical scenario of the dipole approach in transverse momentum representation, we perform predictions for the D-meson production focusing on high energy pp collisions at the LHC. Moreover, our results take into account large and low p_T-spectrum by considering a wide range of rapidity bins. Both forward and central rapidities are considered for D^0, D^+, and D^{*+} production, as well as the cross section ratios $\sigma(D^+)/\sigma(D^0)$ and $\sigma(D^{*+})/\sigma(D^0)$ at central rapidities. The main novelty is the use of the recently proposed phenomenological parameterization for the UGD based on geometric scaling properties that correctly reproduces the hadron spectrum in pp collisions [26]. It describes the saturated and dilute perturbative QCD regimes and has been successfully extended to heavy-ion collisions [27,28]. Moreover, we consider a simplified "Weizsäcker–Williams" (WW) gluon TMD which has been used in studies of Z^0 hadroproduction [29].

The paper is organized as follows. In Sec. 2 the theoretical framework to obtain the D-meson production in the dipole formalism in transverse momentum representation is presented. In Sec. 3 results are shown for several analytical models for the gluon TMD that are compared to the experimental measurements reported by the ALICE and LHCb Collaborations at the LHC, with the corresponding theoretical uncertainties investigated. At last, in Sec. 4 we summarize our main conclusions and remarks.

2. Theoretical formalism

The charmed meson production is evaluated within the QCD dipole framework, where the basic assumption consists that the production process can be determined by a color dipole, $Q\,\bar{Q}$, interacting with the nucleon/nucleus in the target rest frame. The inclusive production of a $Q\,\bar{Q}$ – originated from virtual gluon fluctuation – is written in terms of the cross section of the process $g + N \to Q\,\bar{Q} + X$, including the superposition of color-singlet and color-octet contributions as well. The hadronic cross section of the process $pp \to Q\,X$ assumes the form

$$\frac{d^4\sigma_{pp\to Q\,\bar{Q}\,X}}{dyd\alpha d^2p_T} = F_g(x_1,\mu_F^2)\,\frac{d^3\sigma_{gp\to Q\,\bar{Q}\,X}}{d\alpha d^2p_T}\,, \tag{1}$$

where y and p_T correspond to the rapidity and transverse momentum of the heavy quark (denoted as Q), respectively, and α ($\bar{\alpha} = 1-\alpha$) is the gluon momentum fraction exchanged with the heavy quark (antiquark). In the expression above the $gp \to Q\,\bar{Q}\,X$ cross section has been convoluted with the projectile gluon UGD. Ignoring the primordial gluon momentum, the quantity $F_g(x_1,\mu_F^2)$ is given by

$$F_g(x_1,\mu_F^2) = \int^{\mu_F^2}\frac{dk_T^2}{k_T^2}\mathcal{F}(x_1,k_T^2)\,. \tag{2}$$

The cross section, as computed in Eq. (1), takes similar form used in the k_T-factorization framework. The heavy quark TMD can be obtained in the momentum representation in terms of the dipole TMD, $\mathcal{T}_{\rm dip}$ [30], in the following way:

$$\begin{aligned}
&\frac{d^3\sigma_{gp\to Q\,\bar{Q}\,X}}{d\alpha d^2p_T}\\
&= \frac{1}{6\pi}\int\frac{d^2\kappa_\perp}{\kappa_\perp^4}\alpha_s(\mu_F^2)\,\mathcal{T}_{\rm dip}(x_2,\kappa_\perp^2)\left\{\left[\frac{9}{8}\mathcal{I}_0(\alpha,\bar{\alpha},p_T)\right.\right.\\
&\left.-\frac{9}{4}\mathcal{I}_1(\alpha,\bar{\alpha},\vec{p}_T,\vec{\kappa}_\perp)+\mathcal{I}_2(\alpha,\bar{\alpha},\vec{p}_T,\vec{\kappa}_\perp)+\frac{1}{8}\mathcal{I}_3(\alpha,\bar{\alpha},\vec{p}_T,\vec{\kappa}_\perp)\right]\\
&\left.+[\alpha\longleftrightarrow\bar{\alpha}]\right\},
\end{aligned} \tag{3}$$

where $\alpha_s(\mu_F^2)$ stands for the running coupling in the one-loop approximation. Also, we have that the auxiliary quantities $\mathcal{I}_i$ ($i = 0,1,2,3$) are given by:

$$\mathcal{I}_0(\alpha,\bar{\alpha},p_T) = \frac{m_Q^2+(\alpha^2+\bar{\alpha}^2)p_T^2}{(p_T^2+m_Q^2)^2}\,, \tag{4}$$

$$\mathcal{I}_1(\alpha,\bar{\alpha},\vec{p}_T,\vec{\kappa}_\perp) = \frac{m_Q^2+(\alpha^2+\bar{\alpha}^2)\vec{p}_T\cdot(\vec{p}_T-\alpha\vec{\kappa}_\perp)}{[(\vec{p}_T-\alpha\vec{\kappa}_\perp)^2+m_Q^2](p_T^2+m_Q^2)}\,, \tag{5}$$

$$\mathcal{I}_2(\alpha,\bar{\alpha},\vec{p}_T,\vec{\kappa}_\perp) = \frac{m_Q^2+(\alpha^2+\bar{\alpha}^2)(\vec{p}_T-\alpha\vec{\kappa}_\perp)^2}{[(\vec{p}_T-\alpha\vec{\kappa}_\perp)^2+m_Q^2]^2}\,, \tag{6}$$

$$\mathcal{I}_3(\alpha,\bar{\alpha},\vec{p}_T,\vec{\kappa}_\perp) = \frac{m_Q^2+(\alpha^2+\bar{\alpha}^2)(\vec{p}_T+\alpha\vec{\kappa}_\perp)\cdot(\vec{p}_T-\bar{\alpha}\vec{\kappa}_\perp)}{[(\vec{p}_T+\alpha\vec{\kappa}_\perp)^2+m_Q^2][(\vec{p}_T-\bar{\alpha}\vec{\kappa}_\perp)^2+m_Q^2]}\,, \tag{7}$$

with m_Q being the heavy quark mass. Moreover, the projectile and target fractional light-cone momentum are denoted by x_1 and x_2, respectively. They are explicitly written in terms of the pair rapidity, $x_{1,2} = \frac{M_{Q\,\bar{Q}}}{\sqrt{s}}\,e^{\pm y}$, where $\sqrt{s}$ is the collision center-of-mass energy and $M_{Q\,\bar{Q}}$ represents the invariant mass of the $Q\,\bar{Q}$ pair,

$$M_{Q\bar{Q}} \simeq 2\sqrt{m_Q^2 + p_T^2}\,. \tag{8}$$

Furthermore, in Eq. (3) $\mathcal{T}_{\rm dip}(x_2, \kappa_\perp^2)$ is the intrinsic dipole TMD that is connected with the dipole cross section $\sigma_{q\bar{q}}$ by means of [31,32]

$$\sigma_{q\bar{q}}(\vec{r}, x) \equiv \frac{2\pi}{3}\int \frac{d^2\kappa_\perp}{\kappa_\perp^4}\left(1 - e^{i\vec{\kappa}_\perp\cdot\vec{r}}\right)\left(1 - e^{-i\vec{\kappa}_\perp\cdot\vec{r}}\right)\mathcal{T}_{\rm dip}(x, \kappa_\perp^2)\,. \tag{9}$$

When the transverse momentum of the gluon target is large enough, such that $\kappa_\perp \gg \Lambda_{\rm QCD}$, a relation between the $k_\perp$-factorization and the dipole approach can be established, implying that the intrinsic dipole TMD can be approximated to the UGD function times α_s. The argument of α_s is given by the gluon transverse momentum. In the D-meson production we can safely apply this approximation since the heavy quark pair production is coupled with small-sized dipoles. This assumption is validated by the range of heavy quark transverse momentum probed experimentally, consequently,

$$\mathcal{T}_{\rm dip}(x_2, \kappa_\perp^2) \simeq \alpha_s\, \mathcal{F}(x_2, \kappa_\perp^2)\,, \tag{10}$$

where $\mathcal{F}(x_2, k_T^2)$ accounts for the target UGD. We shall stress that the relation (10) is not necessarily in the small $\kappa_\perp$ region, which is associated to dipoles of large sizes and where the gluon UGD is not sufficiently constrained.

As pointed previously, there exist several parametrizations for the UGD and here we will use the analytical models proposed in Refs. [33,26,29]. The first model for gluon UGD is derived from a saturated form of the Golec-Biernat and Wüsthoff (GBW) dipole cross section [33] that effective accounts for a scattering of a color dipole off a nucleon [34]

$$\sigma_{q\bar{q}}(r, x) = \sigma_0\left[1 - \exp\left(-\frac{r^2\, Q_s^2}{4}\right)\right], \tag{11}$$

and, by applying the corresponding Fourier transform of the Eq. (9), one arrives the expression:

$$\mathcal{F}_{GBW}(x, k_T^2) = \frac{3\,\sigma_0}{4\pi^2\alpha_s}\frac{k_T^4}{Q_s^2}\exp\left(-\frac{k_T^2}{Q_s^2}\right), \tag{12}$$

where $\alpha_s = 0.2$ and Q_s is the saturation scale, $Q_s^2(x) = (x_0/x)^\lambda$ GeV^2. In this study we use the set of parameters $\sigma_0 = 27.43$ mb, $x_0 = 0.40 \times 10^{-4}$, and $\lambda = 0.248$ that has been determined from the fit done to the recently extracted data on F_2 at low-x given in Ref. [35]. Using the GBW UGD, the quantity $F_g(x_1, \mu_F^2)$ in Eq. (2) can be analytically computed and reads

$$F_g^{GBW}(x_1, \mu_F^2) = \frac{3\sigma_0}{4\pi^2\alpha_s}Q_s^2(x_1)\left[1 - \left(1 + \frac{\mu_F^2}{Q_s^2(x_1)}\right)\exp\left(-\frac{\mu_F^2}{Q_s^2(x_1)}\right)\right]. \tag{13}$$

The second model has been proposed recently by Moriggi, Peccini, and Machado (MPM) [26] taking into account the geometric scaling observed in high p_T hadron production in pp collisions along with a Tsallis-like behavior of measured hadron spectrum, given by:

$$\mathcal{F}_{MPM}(x, k_T^2) = \frac{3\,\sigma_0}{4\pi^2\alpha_s}\frac{(1+\delta n)}{Q_s^2}\frac{k_T^4}{\left(1 + \frac{k_T^2}{Q_s^2}\right)^{(2+\delta n)}}, \tag{14}$$

with the scaling variable being $\tau = k_T^2/Q_s^2$ and $Q_s^2(x) = (x_0/x)^{0.33}$. The function $\delta n = a\tau^b$ defines the power-like behavior of the spectrum of the produced gluons at high momentum. The parameters σ_0, x_0, a, and b are obtained by fitting DIS data at small-x resulting in: $\sigma_0 = 19.75$ mb, $x_0 = 5.05 \times 10^{-5}$, $a = 0.075$ and $b = 0.188$. Moreover, the same fixed value of the strong coupling ($\alpha_s = 0.2$) used in GBW model is considered here.

Finally, the WW model [29] for the gluon distribution, inspired by the Weizsäcker-Williams method of virtual quanta, considers the one-gluon exchange between a point-like parton and a hard probe at large momentum transfer. This gluon exchange plays a role similar with the virtual photon exchange such that the associated virtual gluon density resembles the virtual photon density originated from a point-like charge described by Weizsäcker-Williams approximation. The UGD in this parametrization read as

$$\mathcal{F}_{WW}(x, k_T^2) = \begin{cases} (N_1 k_T^2/k_0^2)(1-x)^7(x^\lambda k_T^2/k_0^2)^{-b} & k_T^2 \geq k_0^2, \\ (N_1 k_T^2/k_0^2)(1-x)^7\, x^{-\lambda b} & k_T^2 < k_0^2, \end{cases} \tag{15}$$

where the normalization constant $N_1 = 0.6$, $k_0 = 1$ GeV, and $\lambda = 0.29$. The factor $(1-x)^7$ accounts for the gluon distribution suppression at large x while the phenomenological parameter b is responsible for controlling the k_T scaling of the gluon distribution. Parametrization above has been used in studies of Lam–Tung relation breaking at the Z^0 hadroproduction in the context of k_T-factorization formalism. It was shown that the shape of WW TMD is crucial for the right description of that relation breaking. In Fig. 1 we show a comparison between the UGDs used in this work and the Kutak-Sapeta (KS) [36] distribution that accounts for nonlinear QCD dynamics. These parameterizations predict distinct behavior on the x and k_T dependences. The UGDs are plotted as a function of k_T for different values of Bjorken variable. At low k_T the UGDs are enhanced and show some suppression as k_T increases. In particular, the suppression observed at large k_T in the GBW model is huge – related to the Gaussian shape present in the dipole cross section – while the KS parametrization provides a power-like behavior. Furthermore, the MPM model present moderate suppression and the WW model has a constant behavior towards larger values of k_T. Additionally, we show the results obtained by integrating the UGDs using Eq. (2) and performing a comparison with some standard DGLAP gluon PDF parametrization. For the latter we considered the MMHT [37] PDF together with its theoretical uncertainty. This allows us to verify the consistency and normalization for the UGDs. In Fig. 2, the $F_g(x, \mu_F)$ is exhibited in terms of x. By considering the uncertainty of the MMHT PDF one verifies that for very low-x the F_g calculated from used UGDs is closer to the DGLAP gluon PDF except the oversimplified GBW parametrization. This similarity is important for the consistency and the applicability of the calculations.

With the purpose of obtaining the D-meson spectra, one has necessarily to assume the hadronization of the heavy quarks via the corresponding fragmentation function, which is interpreted as the probability that a heavy quark fragments into a given heavy meson. Therefore, the D-meson production can be calculated by convoluting the heavy quark cross section with the fragmentation function,

$$\frac{d^3\sigma_{pp\to DX}}{dY d^2P_T} = \int_{z_{\rm min}}^1 \frac{dz}{z^2} D_{Q/D}(z, \mu_F^2)\int_{\alpha_{\rm min}}^1 d\alpha\, \frac{d^4\sigma_{pp\to Q\bar{Q}X}}{dy d\alpha d^2p_T}\,, \tag{16}$$

where z is the fractional momentum of the heavy quark Q carried by the D-meson and $D_{Q/D}(z, \mu_F^2)$ is the fragmentation function. Here we will assume the parametrization proposed in Ref. [38] that includes the DGLAP evolution. Moreover, the quantities m_D, $Y = y$, and P_T are the mass, rapidity, and transverse momentum of the D-meson, respectively [39]. As $z \equiv P_T/p_T$, one can use $p_T = P_T/z$ and the lower limits for the z and α integrations are given by:

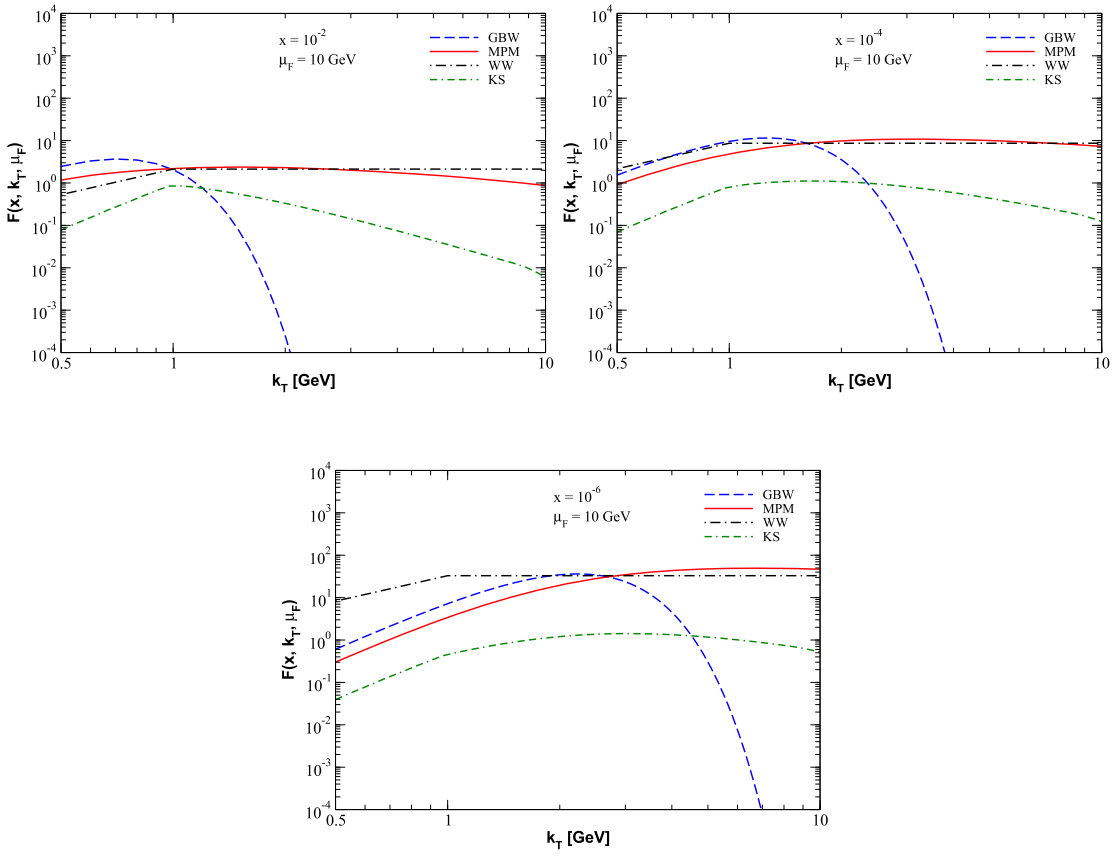

Fig. 1. Comparison between the unintegrated GBW, MPM, WW and KS gluon distributions as a function of k_T for different fixed values of x. The result with the KS parametrization is obtained considering the scale $\mu_F = 10$ GeV.

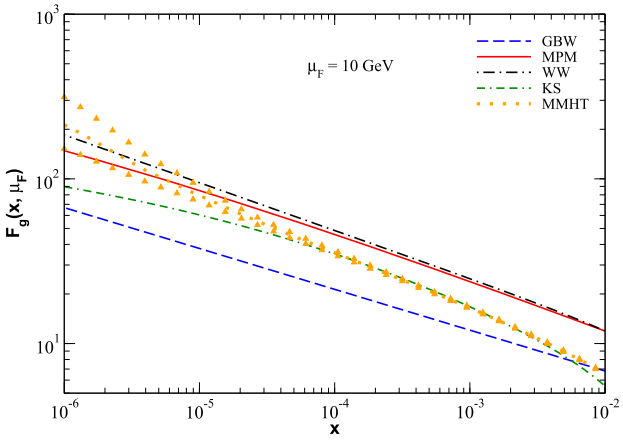

Fig. 2. The dependence on x of the integrated UGD GBW, MPM, WW and KS compared with the MMHT gluon PDF based on the DGLAP evolution equation. The result with the MMHT parametrization is obtained considering the scale $\mu_F = 10$ GeV and the corresponding uncertainty is represented by the triangle symbols.

$$z_{\min} = \frac{\sqrt{m_D^2 + P_T^2}}{\sqrt{s}} e^Y , \tag{17}$$

$$\alpha_{\min} = \frac{z_{\min}}{z} \sqrt{\frac{m_Q^2 z^2 + P_T^2}{m_D^2 + P_T^2}} . \tag{18}$$

The GBW parametrization allows us to obtain an approximate expression for the rapidity and p_T distributions. In the kinematic range considered here the hard scale μ_F is higher than the saturation scale, $\mu_F^2/Q_s^2(x) \gg 1$. In this limit, $F_g^{GBW} \approx 3\sigma_0 Q_s^2(x_1)/(2\pi)^2\alpha_s$. Moreover, at central rapidity, $Y = 0$, the typical value of z_{min} in the range $p_T < 3m_D$ at $\sqrt{s} = 5$ TeV is $z_{min} \sim 2 \times 10^{-3}$. Based on this fact, the lower limit in the α-integration can be safely considered $\alpha_{min} \to 0$. It can be shown that the heavy quark p_T-spectrum is given by:

$$\frac{d^2\sigma(gp \to Q\,\bar{Q}\,X)}{d^2p_T} \approx \frac{3}{5}\frac{\sigma_0 Q_s^2(x_2)}{4(2\pi)^2}\left[\frac{p_T^4 + \frac{25}{9}m_c^2 p_T^2 + m_c^4}{(m_c^2 + p_T^2)^4}\right] . \tag{19}$$

Instead of integrating over z in Eq. (16), we will compute the cross section using a simplification for the fragmentation function, $D_c(z, \mu_F) \sim \delta(z - \langle z\rangle_c)$. The average momentum fraction $\langle z\rangle_c$ is defined as [38],

$$\langle z\rangle_c(\mu_F) = \frac{1}{B_c(\mu_F)} \int_{z_{cut}}^{1} dz z D_c(z, \mu_F), \quad \text{with}$$

$$B_c(\mu_F) = \int_{z_{cut}}^{1} dz D_c(z, \mu_F), \tag{20}$$

where B_c is the branching fraction $c \to D$ and $z_{cut} = 0.1$ [38]. For the KKKS fragmentation function considered here, one has $\langle z\rangle_c(\mu_F = 2m_c) = 0.573, 0.571$, and 0.617 for D^0, D^+ and D^{*+}, respectively. The average fraction is weakly dependent on the hard scale μ_F, with a $\sim 20\%$ decreasing at $\mu_F = m_Z$. Therefore, we will take $\langle z\rangle \equiv \langle z\rangle_c(2m_c)$ and the meson spectrum will be given by

$$\frac{d^3\sigma_{pp\to DX}}{dY d^2P_T} \approx \left[\frac{\langle z\rangle\,\sigma_0}{2(2\pi)^2}\right]^2 \frac{Q_s^2(x_1)Q_s^2(x_2)}{5}$$

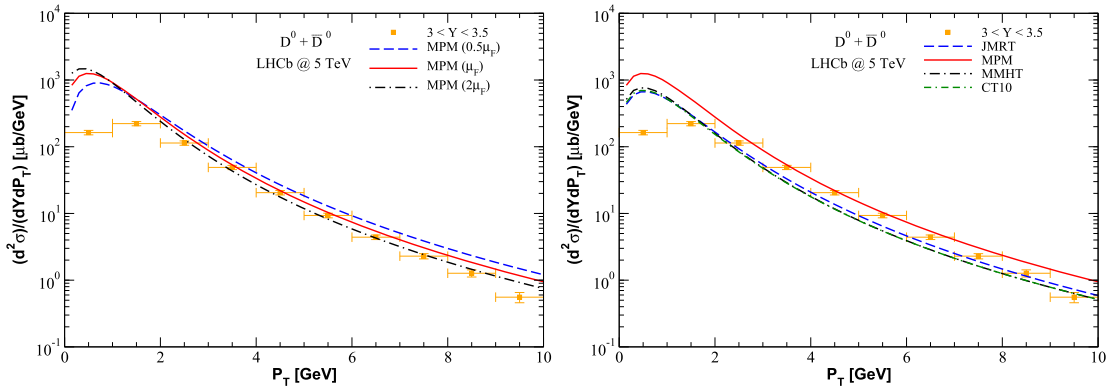

Fig. 3. Comparison regarding the uncertainties on the factorization scale (left panel) as well as the integrated MPM UGD and the JMRT [41], MMHT [37] and CT10 [42] PDFs (right panel). The results take into account the D^0 meson production cross section measured in pp collisions at the LHCb experiment [40] in the kinematic region of $\sqrt{s} = 5$ TeV and rapidity range, $3 < Y < 3.5$.

$$\times \left[\frac{9m_c^4\langle z\rangle^4 + 25m_c^2\langle z\rangle^2 P_T^2 + 9P_T^4}{(m_c^2\langle z\rangle^2 + P_T^2)^4} \right]. \qquad (21)$$

In what follows we take the previously discussed UGD parameterizations to calculate the D-meson production in pp collisions and performed a comparison with the respective experimental measurements obtained at the LHC.

3. Results and discussions

Let us present the results obtained with the dipole approach in transverse momentum representation and using three parametrizations for the UGD introduced before, namely the GBW, MPM, and WW models. Considering the D-meson production in high energy hadron-hadron collisions we predict the distributions in transverse momentum and rapidity focusing in the LHC kinematic regime. Our results are directly compared to the experimental data reported by ALICE and LHCb Collaborations.

In order to evaluate the uncertainties concerning the theoretical calculations, we perform an analysis regarding the perturbative uncertainty related to the factorization scale and also between the integrated UGD and the PDFs. Our analysis is associated to the D^0 measurement in pp collisions performed at the LHCb experiment [40] considering center-of-mass energy of 5 TeV and rapidity interval, $3 < Y < 3.5$. In Fig. 3 (left panel) we show the results with MPM model assuming three choices of the factorization scale, that is, $0.5\mu_F$, μ_F, and $2\mu_F$. The difference between the results is more apparent for large P_T, where one has $\sim 20\%$ deviation regarding the prediction MPM(μ_F) with the central value of the factorization scale. Besides, it is not possible strongly discriminate between the results and the data. On the other hand, the Fig. 3 (right panel) shows the predictions for the integrated MPM UGD and the collinear PDF parameterizations JMRT [41], MMHT [37], and CT10 [42]. One can verify that the main effect of using integrated UGD versus a collinear gluon PDF is the overall normalization. This is expected and can be traced back considering the results presented in Fig. 2, where the corresponding differences for F_g are converted into the results for the cross section. Moreover, the result with MPM fairly describes the experimental data. An appropriated choice of factorization scale and/or charm mass can bring the MPM prediction closer to those using standard gluon distribution.

In Fig. 4 we show the results for D^0, D^+, and D^{*+} production including the charge conjugates states in pp collisions at $\sqrt{s} = 5$ TeV. The predictions for the differential cross section are confronted against the measurements from the LHCb Collaboration [40] considering three distinct rapidity bins: $2 < Y < 2.5$, $3 < Y < 3.5$, and $4 < Y < 4.5$. Selecting all the three D-meson and rapidity bins considered here, we can verify that the MPM and WW parametrizations give quite similar results at $P_T < 4$ GeV and both models are in good agreement with the experimental measurements, except for $P_T < 2$ GeV. Moreover, a small difference between MPM and WW results appears, taking the spectrum from $P_T > 4$ GeV. This difference is a bit more pronounced at very forward rapidity interval, $4 < Y < 4.5$, where such models are not in completely agreement to the correct normalization of the P_T spectrum. In contrast, the GBW parameterization describes the experimental measurements in a narrow P_T distribution, $2 < P_T < 3$ GeV, where it provides a better agreement at very forward rapidity. Apart from the particular P_T spectrum mentioned before, the GBW results is loosing adherence to data. The reason for this behavior consists in the Gaussian shape present in the GBW approach that enters in Eqs. (10) and (12), leading to the suppression pattern observed in the results. For sake of comparison, we show the results taking into account the approximate expression for the D-meson spectrum given in Eq. (21) (labeled APPROX hereafter). For D^0 case, only the measurement at $4 < Y < 4.5$ can be reasonably described. However, considering the D^+ and D^{*+} production, the predictions are in good agreement with the experimental data at the region $3 < Y < 3.5$. In these case, the approximate expression mimics the results from MPM or the WW UGDs. Although the simple form, this approximated expression is able to reproduce the results regarding the complete calculation with the UGDs considering some particular cases, which is a surprising result given the simplicity of the analytical expression derived within the color dipole formalism. Furthermore, in order to clarify the description of the data by the UGDs models, the ratio data/theory is presented considering the MPM parameterization and the rapidity interval $3 < Y < 3.5$.

In Fig. 5 we present the numerical results at the center-of-mass energy of $\sqrt{s} = 13$ TeV for the differential cross section and the ratio data/theory that considers the same D-mesons and rapidity bins analyzed previously in comparison to the experimental data provided by the LHCb experiment [43]. We can notice the same pattern observed at $\sqrt{s} = 5$ TeV, however the predictions with MPM and WW present some difference as the P_T spectrum increases, specially in the $2 < Y < 2.5$ and $4 < Y < 4.5$ rapidity bins. Moreover, the MPM and WW parameterizations present a significant improvement concerning the description of the experimental data in the very forward rapidity kinematic region. Additionally, we found that the same similarities with GBW results at $\sqrt{s} = 5$ TeV.

In the following an analysis of the D^0, D^+, and D^{*+} production in pp collisions at midrapidity region is done. The corresponding theoretical predictions for the double-differential cross section (including the ratio data/theory) at 5.02 TeV in terms of P_T and Y are displayed in Fig. 6, where the results are compared with the data collected by the ALICE Collaboration [44,45]. Apparently, the

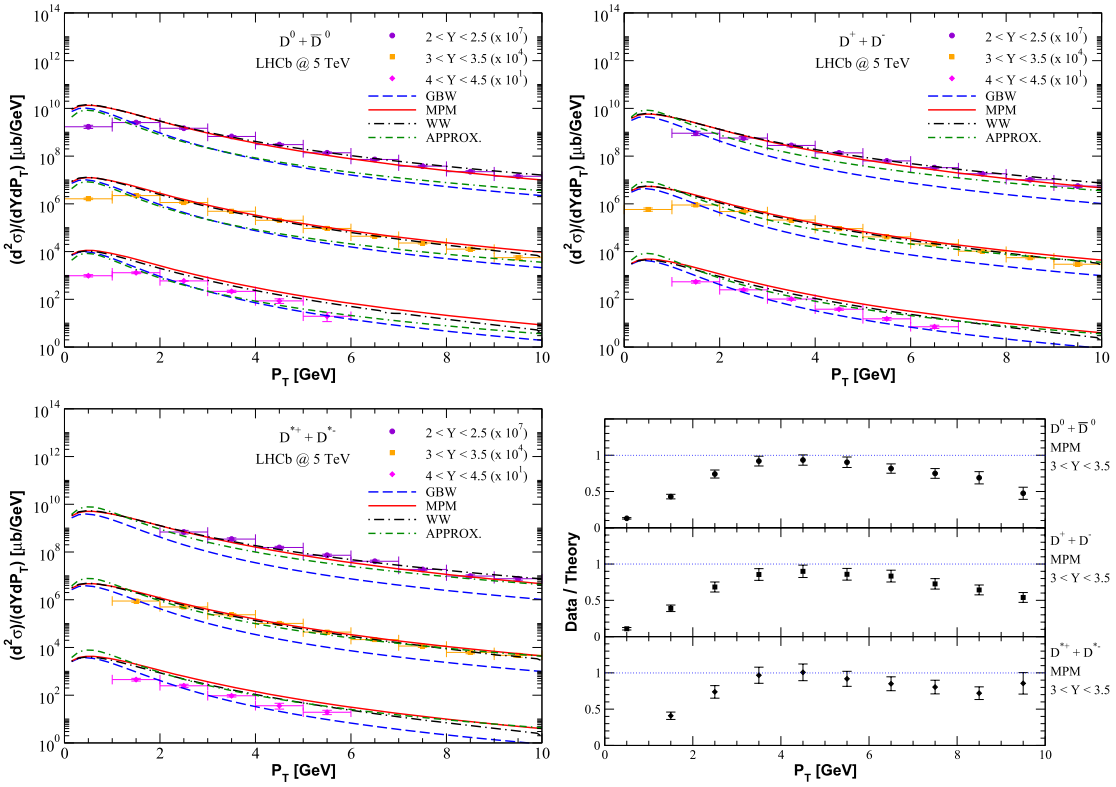

Fig. 4. Double-differential cross sections for D^0 (left panel), D^+ (right panel) and D^{*+} (bottom panel) production in pp collisions at $\sqrt{s} = 5$ TeV considering three forward rapidity bins. The results are obtained using the GBW, MPM, and WW parameterizations as well as the approximate relation obtained in Eq. (21). Moreover, the ratio data/theory is presented. The corresponding comparison is performed with the measurements from the LHCb experiment [40].

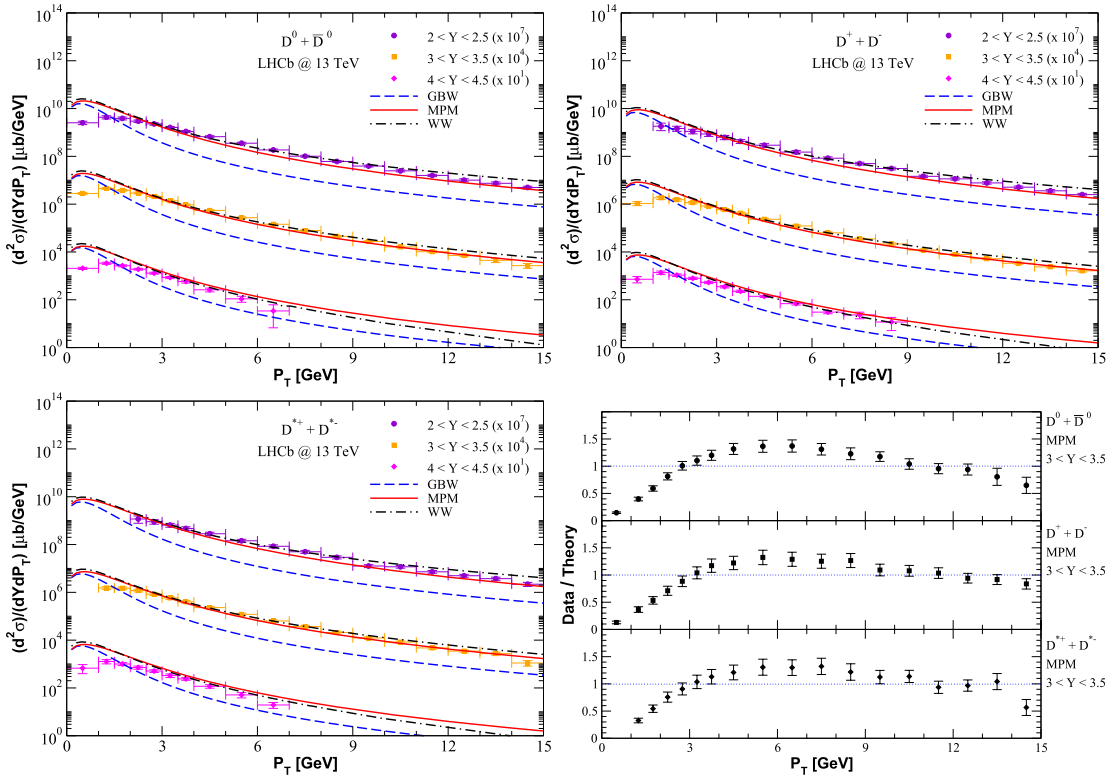

Fig. 5. Double-differential cross sections for D^0 (left panel), D^+ (right panel), and D^{*+} (bottom panel) production in pp collisions at $\sqrt{s} = 13$ TeV considering three forward rapidity bins. The results are obtained using the GBW, MPM, and WW parameterizations. Moreover, the ratio data/theory is presented. The corresponding comparison is performed with the measurements from the LHCb experiment [43].

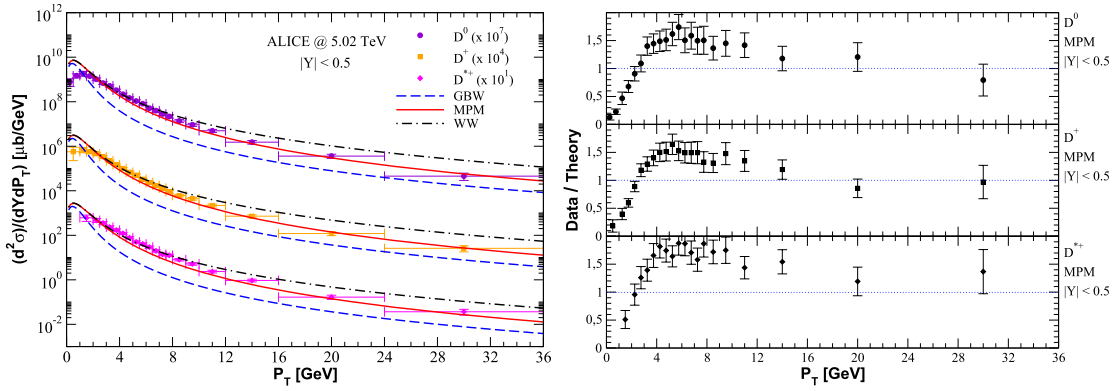

Fig. 6. Double-differential cross sections and the ratio data/theory for D^0, D^+, and D^{*+} production in pp collisions at $\sqrt{s} = 5.02$ TeV at midrapidity region. The results are obtained using the GBW, MPM, and WW parametrizations and compared to the experimental measurements from the ALICE experiment [44,45].

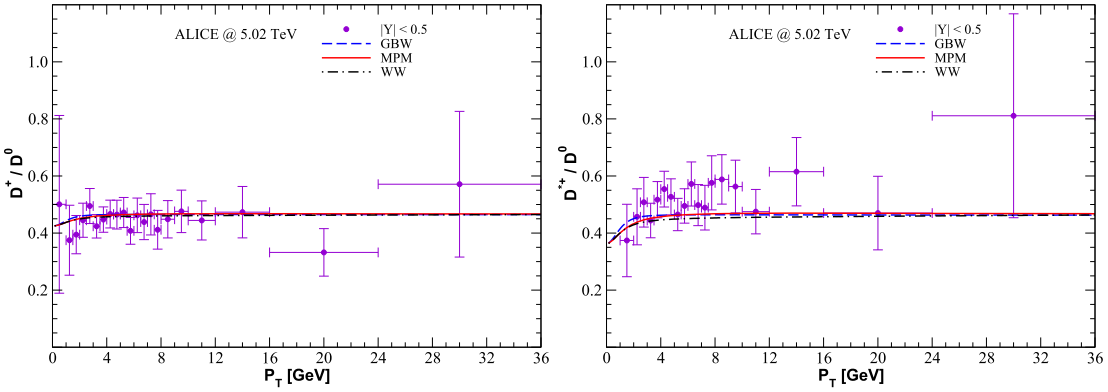

Fig. 7. Ratios between the D^+/D^0 (left panel) and D^{*+}/D^0 (right panel) differential production cross sections in terms of P_T. The results are obtained using the GBW, MPM, and WW parametrizations and compared to the experimental measurements from the ALICE experiment [44,45].

WW model predictions fairly reproduce the experimental data at low P_T spectrum, while the GBW approach underestimates the experimental measurements. We can also observe that the WW estimates begin deviate from the measurements towards large values of P_T by overshooting them, whereas the MPM results do a better job at describing the data considering the large P_T distribution. Then, we can conclude that the WW and MPM parametrizations are able to provide a reasonable description of the measurements performed by the ALICE experiment at central rapidity regarding the low and large P_T distribution, respectively. In addition, we present the ratios of the differential cross sections of D^0, D^+, and D^{*+} mesons produced in pp collisions at $\sqrt{s} = 5.02$ TeV and $Y = 0$ also obtained by the ALICE Collaboration [44,45]. In particular, the ratios D^+/D^0 and D^{*+}/D^0 as a function of P_T are shown in Fig. 7. One can see that the ratios between the corresponding D-meson cross section do not provide an evidence of strong P_T dependence, instead showing a constant behavior through the P_T spectrum. This fact indicates that we can not identify discriminatory differences particularly between the fragmentation functions of charm quarks to D^0, D^+, and D^{*+} mesons. Along with these considerations we can add that the GBW, MPM, and WW predictions are in agreement with the measurements within the experimental uncertainties and we have no basis to distinguish the three UGD parametrizations. In the approximate expression, Eq. (21), the ratio R_{M_1/M_2} scales with $\left(\langle z\rangle_{M_1}/\langle z\rangle_{M_2}\right)^{2(1+\lambda)}$ at large P_T and central rapidity $Y = 0$.

Finally, the predictions for the differential cross section of D^0 production as a function of the rapidity distribution are shown in Fig. 8. The MPM results are confronted with the pp data assuming the kinematic region achieved by the ALICE [44,45] and LHCb [40]

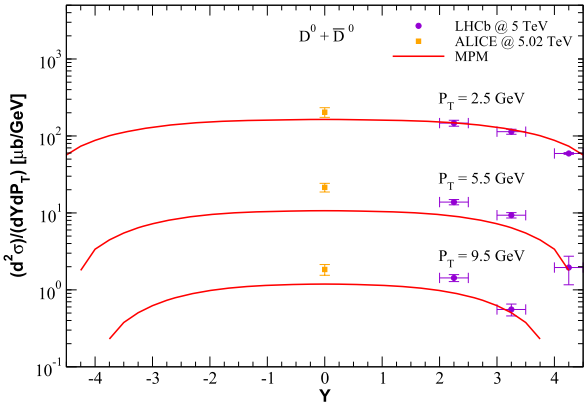

Fig. 8. Double-differential cross sections as a function of the rapidity distribution for D^0 production in pp collisions considering three values of the momentum distribution. The results are obtained with MPM parameterization and compared with the measurements from the ALICE [44,45] and LHCb [40] experiments.

experiments taking three values of P_T: $P_T = 2.5, 5.5$, and 9 GeV. We observe that the results are symmetric with respect to central rapidity, $Y = 0$, which is covered by ALICE measurement. This is expected because the projectile and target are identical, generating the symmetry seen in the rapidity distribution associated to the particle production in the projectile side and in the target side. In addition, the MPM predictions present a better description of data in the forward rapidity kinematic region covered by the LHCb detector.

Besides, the x_2 probed in the kinematic ranges determined by the ALICE and LHCb experiments has to be investigated, specially

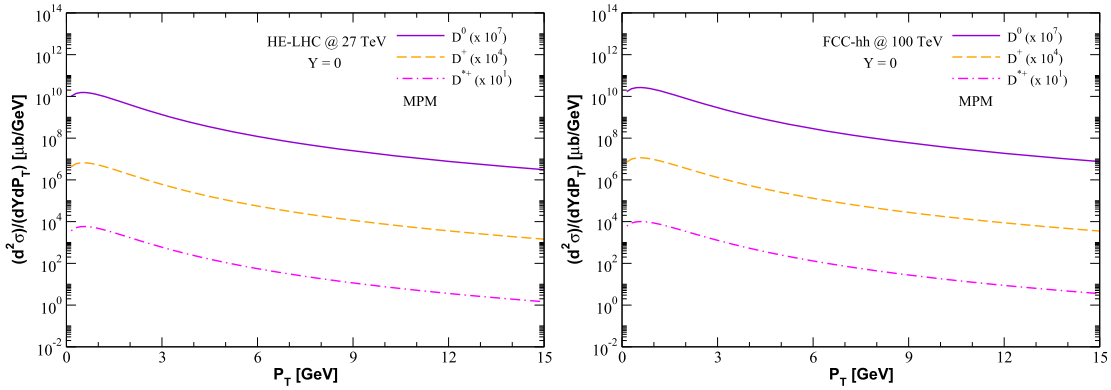

Fig. 9. Double-differential cross sections for D^0, D^+, and D^{*+} production in pp collisions at the HE-LHC ($\sqrt{s} = 27$ TeV, left panel) and FCC-hh ($\sqrt{s} = 100$ TeV, right panel) at midrapidity region. The results are obtained using the MPM parametrization.

in the very forward ($4 < Y < 4.5$) and central ($|Y| < 0.5$) rapidity bins. We have that the mean value of $\langle x_2 \rangle$ achieved at the LHCb experiment at 5 and 13 TeV corresponds to $\langle x_2 \rangle \sim 3 \times 10^{-5}$ and $\langle x_2 \rangle \sim 2 \times 10^{-5}$, respectively, while at the ALICE experiment at 5.02 TeV this value is $\langle x_2 \rangle \sim 7 \times 10^{-3}$. Clearly, these results for $\langle x_2 \rangle$ ensure that we perform predictions within the limit of validity of dipole formalism, $x_2 \leq 10^{-2}$. Therefore, the color dipole framework is particularly suitable for small x_2 values since most parametrizations of the dipole cross section are fitted (their parameters) only to DIS data with Bjorken-$x \leq 0.01$. Here, all data sets provided by the ALICE and LHCb experiments are within the threshold of validity of the color dipole approach, see, e.g., the $\langle x_2 \rangle$ values discussed previously, allowing us to employ such formalism to analyze the corresponding experimental measurements of the D-meson production in pp collisions.

As a matter of completeness, we provide predictions for D-meson production concerning the pp collisions aiming the proposals of center-of-mass energies in future colliders. In particular, the High-Energy Large Hadron Collider (HE-LHC) [46] and the Future Circular Collider (FCC-hh) [47] are expected to achieve colliding energies of $\sqrt{s} = 27$ TeV and 100 TeV, respectively. The results corresponding for D^0, D^+, and D^{*+} with the MPM approach are found in Fig. 9. Future experimental measurements of D-meson production can be fruitful in order to extend the probed kinematic region and to complement our approaches based on QCD dynamics such as color dipole formalism, as well as the underlying assumptions considered in the gluon TMD. Along with this aspects the HE-LHC and the FCC-hh could enable us to perform further investigations.

4. Summary

We investigated the D-meson production at high energy pp collisions within the color dipole framework, where we employ three distinct parametrizations for the unintegrated gluon distribution. We provide predictions for the D^0, D^+, and D^{*+} double-differential cross section that are directly compared to the most recent data reported by the LHC experiments. We have verified that the MPM and WW results are able to reasonable describe the transverse momentum and rapidity distributions of the experimental measurements obtained by the ALICE and LHCb Collaborations. In particular, at central rapidity, WW and MPM predictions can better reproduce the data concerning low and large P_T spectrum, respectively. On the other hand, we have found out that the GBW parametrization undershoots the experimental data provided by ALICE and LHCb experiments. In general, better results are given with the MPM approach even at large P_T domain. We have demonstrated that the treatment of the D-meson production at high energies can be appropriately formulated in the color dipole framework where the corresponding results are parameter free.

In view of the trend found in the MPM and WW results obtained in this analysis, the new data taking from the future colliders in pp mode will be valuable to extend the kinematic region and to improve the MPM and WW parametrizations for the unintegrated gluon distribution.

Declaration of competing interest

The authors declare the following financial interests/personal relationships which may be considered as potential competing interests:

G. Gil da Silveira reports was provided by National Council for Scientific and Technological Development. Magno Machado reports was provided by National Council for Scientific and Technological Development. Glauber Sampaio dos Santos reports was provided by Coordination of Higher Education Personnel Improvement.

Data availability

No data was used for the research described in the article.

Acknowledgements

This work was partially financed by the Brazilian funding agencies CAPES, CNPq, and FAPERGS. This study was financed in part by the Coordenação de Aperfeiçoamento de Pessoal de Nível Superior - Brasil (CAPES) - Finance Code 001. GGS acknowledges funding from the Brazilian agency Conselho Nacional de Desenvolvimento Científico e Tecnológico (CNPq) with grant 311851/2020-7.

References

[1] G. Goldhaber, J.E. Wiss, Annu. Rev. Nucl. Part. Sci. 30 (1980) 337.
[2] G. Goldhaber, et al., Phys. Rev. Lett. 37 (1976) 255.
[3] I. Peruzzi, et al., Phys. Rev. Lett. 37 (1976) 569.
[4] A. Andronic, et al., Eur. Phys. J. C 76 (2016) 107.
[5] F. Prino, R. Rapp, J. Phys. G 43 (2016) 093002.
[6] J.C. Collins, D.E. Soper, G.F. Sterman, Adv. Ser. Dir. High Energy Phys. 5 (1989) 1.
[7] L.V. Gribov, E.M. Levin, M.G. Ryskin, Phys. Rep. 100 (1983) 1.
[8] G. Marchesini, B.R. Webber, Nucl. Phys. B 310 (1988) 461.
[9] E.M. Levin, M.G. Ryskin, Phys. Rep. 189 (1990) 268.
[10] S. Catani, M. Ciafaloni, F. Hautmann, Phys. Lett. B 242 (1990) 97; Nucl. Phys. B 366 (1991) 135.
[11] B.A. Kniehl, G. Kramer, I. Schienbein, H. Spiesberger, Phys. Rev. D 71 (2005) 014018; Eur. Phys. J. C 41 (2005) 199; Eur. Phys. J. C 72 (2012) 2082.
[12] I. Helenius, H. Paukkunen, J. High Energy Phys. 05 (2018) 196.
[13] M. Cacciari, M. Greco, P. Nason, J. High Energy Phys. 05 (1998).
[14] M. Cacciari, S. Frixione, N. Houdeau, M.L. Mangano, P. Nason, G. Ridolfi, J. High Energy Phys. 10 (2012).

[15] M.G. Ryskin, A.G. Shuvaev, Yu.M. Shabelski, Phys. At. Nucl. 64 (2001) 120; Yad. Fiz. 64 (2001) 123; Phys. At. Nucl. 64 (2001) 1995; Yad. Fiz. 64 (2001) 2080.
[16] D. Kharzeev, K. Tuchin, Nucl. Phys. A 735 (2004) 248.
[17] Yu.M. Shabelski, A.G. Shuvaev, Phys. At. Nucl. 69 (2006) 314.
[18] M. Luszczak, R. Maciula, A. Szczurek, Phys. Rev. D 79 (2009) 034009.
[19] R. Maciula, A. Szczurek, Phys. Rev. D 87 (2013) 094022.
[20] G. Chachamis, M. Deák, M. Hentschinski, G. Rodrigo, A. Sabio Vera, J. High Energy Phys. 1509 (2015) 123.
[21] V.P. Goncalves, F.S. Navarra, Nucl. Phys. A 842 (2010) 59.
[22] F. Carvalho, A.V. Giannini, V.P. Goncalves, F.S. Navarra, Phys. Rev. D 96 (2017) 094002.
[23] R. Angeles-Martinez, et al., Acta Phys. Pol. B 46 (2015) 2501.
[24] N.N. Nikolaev, G. Piller, B.G. Zakharov, Zh. Eksp. Teor. Fiz. 108 (1995) 1554; J. Exp. Theor. Phys. 81 (1995) 851; Z. Phys. A 354 (1996) 99.
[25] J. Raufeisen, J.C. Peng, Phys. Rev. D 67 (2003) 054008.
[26] L.S. Moriggi, G.M. Peccini, M.V.T. Machado, Phys. Rev. D 102 (2020) 034016.
[27] L.S. Moriggi, G.M. Peccini, M.V.T. Machado, Phys. Rev. D 103 (3) (2021) 034025.
[28] G.M. Peccini, L.S. Moriggi, M.V.T. Machado, Phys. Rev. D 103 (2021) 054009.
[29] L. Motyka, M. Sadzikowski, T. Stebel, Phys. Rev. D 95 (2017) 114025.
[30] V.P. Goncalves, B. Kopeliovich, J. Nemchik, R. Pasechnik, I. Potashnikova, Phys. Rev. D 96 (2017) 014010.
[31] N.N. Nikolaev, B.G. Zakharov, Z. Phys. C 49 (1991) 607.
[32] J. Bartels, K.J. Golec-Biernat, H. Kowalski, Phys. Rev. D 66 (2002) 014001.
[33] K.J. Golec-Biernat, M. Wüsthoff, Phys. Rev. D 60 (1999) 114023.
[34] K.J. Golec-Biernat, M. Wusthoff, Phys. Rev. D 59 (1998) 014017.
[35] K. Golec-Biernat, S. Sapeta, J. High Energy Phys. 1803 (2018) 102.
[36] K. Kutak, S. Sapeta, Phys. Rev. D 86 (2012) 094043.
[37] L.A. Harland-Lang, A.D. Martin, P. Motylinski, R.S. Thorne, Eur. Phys. J. C 75 (2015) 204.
[38] T. Kneesch, B.A. Kniehl, G. Kramer, I. Schienbein, Nucl. Phys. B 799 (2008) 34.
[39] R. Maciula, A. Szczurek, Phys. Rev. D 87 (2013) 094022.
[40] R. Aaij, et al., LHCb Collaboration, J. High Energy Phys. 06 (2017) 147.
[41] S.P. Jones, A.D. Martin, M.G. Ryskin, T. Teubner, J. Phys. G 44 (2017) 03LT01.
[42] H.L. Lai, M. Guzzi, J. Huston, Z. Li, P.M. Nadolsky, J. Pumplin, C.P. Yuan, Phys. Rev. D 82 (2010) 074024.
[43] R. Aaij, et al., LHCb Collaboration, J. High Energy Phys. 03 (2016) 159, erratum: J. High Energy Phys. 09 (2016) 013, erratum: J. High Energy Phys. 05 (2017) 074.
[44] S. Acharya, et al., ALICE Collaboration, Eur. Phys. J. C 79 (2019) 388.
[45] S. Acharya, et al., ALICE Collaboration, J. High Energy Phys. 05 (2021) 220.
[46] A. Abada, et al., Eur. Phys. J. Spec. Top. 228 (2019) 1109.
[47] A. Abada, et al., Eur. Phys. J. Spec. Top. 228 (2019) 755.